Northern Hemisphere ice sheets and ocean interactions during the last glacial period in a coupled ice sheet-climate model

Louise Abot[1], Aurélien Quiquet[2], and Claire Waelbroeck[1]

[1]LOCEAN/IPSL, Sorbonne Université-CNRS-IRD-MNHN, UMR7159, 75005 Paris, France
[2]LSCE/IPSL, CEA-CNRS-UVSQ, Université Paris-Saclay, UMR8212, 91190 Saint-Aubin, France

Correspondence: Louise Abot (louise.abot@locean.ipsl.fr)

Abstract. This study examines the interactions between the Northern Hemisphere ice sheets and the ocean during the last glacial period. We explore the consequences of an ocean subsurface warming on ice sheet dynamics and the associated feedbacks, using the climate model of intermediate complexity iLOVECLIM coupled with the ice sheet model GRISLI. Our study shows that amplified oceanic basal melt rates lead to significant freshwater release from both increased calving and basal melt fluxes. Inland, dynamic thinning occurs over the Eurasian and Iceland ice sheets, leading to destabilization, while the coasts of Greenland and the eastern part of the Laurentide ice sheet are thickening. There, the increased oceanic basal melt rates lead to a reduction in the thickness of the ice shelves and the ice flow at the grounding line, resulting in upstream accumulation. Nevertheless, the influx of fresh water temporarily increases sea-ice extent, reduces convection in the Labrador Sea, weakens the Atlantic meridional overturning circulation, lowers surface temperatures in the Northern Hemisphere and increases the subsurface temperatures in the Nordic Seas. The release of cold and fresh water leads to a decrease in ice sheet discharge (negative feedback) for the Greenland and Eurasian ice sheets. The Laurentide ice sheet is rather stable due to low background temperatures and salinity at shelf drafts in the Baffin Bay and Labrador Sea in the model. Still, we show that we are able to trigger a grounding line retreat by imposing ad-hoc oceanic melt rates (10 m/yr). However, continental ice loss stops as soon as we halt the perturbation. This study emphasizes the complex feedback mechanisms at the ocean-ice sheet interface, stressing the necessity for more accurately constrained model results to enhance our understanding of past changes and the predictions of future ice sheet behaviour and sea level rise.

1 Introduction

Recent studies of the Antarctic ice sheet show that warm oceanic water plays an important role in continental ice thinning, impacting not only floating but also grounded ice (e.g., Pritchard et al., 2012; Reese et al., 2018; Gudmundsson et al., 2019)). The increase of ocean sub-shelf melt rates induces a thinning and eventually break up of the ice shelves, reducing the buttressing effect. This results in an acceleration of the ice flow upstream and a dynamic thinning of the ice sheet inland. The ongoing warming of the ocean (Johnson and Lyman, 2020) could lead to the collapse of the West Antarctic Ice Sheet, among other dramatic consequences, amplifying the sea level rise (Joughin and Alley, 2011; Naughten et al., 2023). To the north, the

Climate of the Past Discussions — Open Access — EGU

Greenland ice sheet's last floating ice tongue also undergoes a thinning driven by warmer ocean temperatures (Wekerle et al.,
25 2024).

Similarly, a number of studies suggests that ocean subsurface warming during the Last Glacial Period ($\approx$ 70-20 years
B.P.), could have destabilized ice sheets and led to massive iceberg discharges (e.g., Shaffer et al., 2004; Marcott et al., 2011;
Max et al., 2022). This period features rapid climate fluctuations that were revealed in Greenland ice cores during the 80s
and that reflect millennial scale variability of the climate system (Dansgaard et al., 1984, 1993). The climate transitioned
30 between relatively cold (stadial) and warm (interstadial) periods in the Northern Hemisphere (Johnsen et al., 1992). Some of
the cold periods are accompanied by massive iceberg discharges in the North Atlantic Ocean. These are identified in marine
sediment cores by one or several layers of ice rafted debris, the materials entrapped and transported by drifting ice (Bond
et al., 1992; Bond and Lotti, 1995; Elliot et al., 1998). Barker et al. (2015), through the examination of a site southwest of
Iceland, suggested that iceberg discharges were a consequence of prolonged stadial conditions rather than a cause. Alvarez-
35 Solas et al. (2010) have proposed that fluctuations of the oceanic temperatures could have triggered Northern Hemisphere ice
sheets surges (i.e., an unsteady state of the ice stream associated with rapid ice flow and dynamic thinning of the ice sheet
inland) and iceberg discharges during this past period. Forcing the Laurentide ice sheet and Hudson stream with an oceanic
warming index during the last glacial period results in the collapse of buttressed ice shelves and subsequent acceleration of
inland ice streams (Alvarez-Solas et al., 2013). Isostatic adjustment may then allow the regrowth of the ice sheet (Bassis et al.,
40 2017). Modelling results suggest that ocean temperature increases can also trigger or amplify ice discharges from the Eurasian
and Greenland ice sheets (Alvarez-Solas et al., 2019; Tabone et al., 2019). However, in these studies, the ocean is considered
as a forcing and as such does not allow to fully capture the interplay between ocean and ice sheets.

Indeed, grasping the response of the entire ice sheet to an oceanic perturbation, or the subsequent oceanic changes following
an influx of continental water, is complex due to the presence of numerous feedback mechanisms at the ocean-ice sheet
45 interface (Goosse et al., 2018; Holland et al., 2020). For instance, under warming conditions, initial ice sheet melting releases
cold and fresh water at the surface, which can lead to negative feedback on climate (Swingedouw et al., 2008; Li et al., 2024).
Additionally, ocean-driven ice shelf thinning may raise the depth-dependent freezing temperature at the ice–ocean interface,
reducing oceanic basal melt rates (Van Achter et al., 2023). Yet freshwater release can also increases stratification, eventually
leading to transient subsurface warming that amplifies oceanic basal melting (Moorman et al., 2020; Li et al., 2024).

50 Here, we take advantage of the climate model of intermediate complexity iLOVECLIM coupled to the ice sheet model
GRISLI to address the following questions : How does ocean subsurface warming at characteristic ice shelves draft affect the
ice sheets dynamics? How does the continental ice melt release affect in turn oceanic circulation, hydrography and ice sheet
dynamics? In this work, we impose abrupt oceanic subsurface warming to the Northern Hemisphere ice sheets to get insights
on both past climate variability and mechanisms at play at the ocean-ice sheet interface.

2 Model and methods

2.1 Climate and ice sheet model

2.1.1 iLOVECLIM

For this study, we use the coupled climate model of intermediate complexity iLOVECLIM which is a code fork of LOVECLIM version 1.2 (Goosse et al., 2010). The core of the model includes oceanic, atmospheric and vegetation components (namely CLIO, EcBilt and VECODE). The model has been used for a wide range of climate studies, from the last million years to the Holocene (e.g., Caley et al., 2014; Bouttes et al., 2018; Arthur et al., 2023). We remind here some of its main features. CLIO is a free surface ocean general circulation model solved on a spherical grid with 3° latitude and longitude resolution and 20 irregular levels in z-coordinates. It includes a thermodynamic sea-ice component (Fichefet and Maqueda, 1997). EcBilt is a quasi-geostrophic atmospheric model solved on a T21 spectral grid with a resolution of 5.6^o in both latitude and longitude. It includes 3 vertical levels at 800, 500 and 200 hPa. VECODE is a dynamic vegetation and carbon allocation model. Major model parameters are listed in Supplementary Tables S1a-c.

2.1.2 GRISLI

iLOVECLIM is coupled to the dynamic ice sheet model GRISLI, which is a 3D thermomechanically coupled ice sheet model that is used here on a cartesian grid of the Northern Hemisphere at 40 km resolution. The equations are described in Ritz et al. (2001) and Quiquet et al. (2018). They are written under shallow ice and shallow shelf approximations. The deformation is calculated using the Glen flow law with an enhancement factor to account for anisotropy. The basal drag is directly proportional to the basal velocities over the grounded ice sheet, while it is zero for the floating ice shelves. The floating ice calves if its thickness falls below the critical threshold of 250 m and the shelves can not extend over the deep ocean. The grounding line formulation follows Tsai and Gudmundsson (2015), and its position is determined by interpolating between the last grounded and the first floating grid cells. Glacial isostatic adjustment is accounted for using an elastic-lithosphere-relaxed-asthenosphere model with a relaxation time of 3000 y (Le Meur and Huybrechts, 1996).

2.1.3 Coupling

The coupling procedure is described in Roche et al. (2014) and Quiquet et al. (2021). In iLOVECLIM, the atmospheric model ECBilt includes an online downscaling (Quiquet et al., 2018). At each atmospheric timestep, temperature and precipitation are computed on the finer resolution GRISLI grid using the standard ECBilt energy and moisture equations. This subgrid information is fed into an Insolation Temperature Melt (ITM, Pollard, 1980; Van Den Berg et al., 2008) model to compute surface mass balance every four hours. The yearly average surface mass balance and surface temperature are then used by GRISLI. In turn, ECbilt receives the yearly topography and ice mask data from GRISLI.

The continental ice melt fluxes are computed in GRISLI each year. These are distributed to the oceanic model over the following year. For the grounded ice sheet, surface melt is routed to the nearest oceanic grid cell following surface topography

while the oceanic basal melt and the calving flux are transferred at the ocean surface where they occur. The local latent heat flux associated with the calving flux and that corresponds to the melting of icebergs by the ocean, is taken into account and the ocean temperatures are adjusted. More details about the freshwater coupling are given in Supplementary Text S2.

The oceanic basal melt rate (OBM) is parameterized as a quadratic function of ocean temperatures (Holland et al., 2008; Favier et al., 2019). When the local ocean temperature is above the freezing temperature, the oceanic basal melt rate is derived as:

$$OBM = \gamma_T * A * (T - T_f)^2 \tag{1}$$

Were the local freezing temperature (T_f) is a function of salinity (Millero, 1978). $A = (\frac{\rho_0 C_{p0}}{L\rho_i})^2 \ K^{-2}$ is a constant depending on physical parameters, whith $\rho_0 = 1030$ kg/m^3 and $C_{p0} = 4002$ J/kg/K the density and specific heat capacity of seawater, $L\rho_i = 300.33 \ 10^6$ J/m^3 the latent heat of fusion of ice times the ice density. γ_T is a tuned parameter that accounts for the heat transfer velocity, and that has been calibrated for this study to $1.09 * 10^{-5}$ m/s. The OBM is computed in the ocean model each day and integrated over each year as the time step for the dynamic ice sheet model is annual. For each horizontal grid point, the rate is calculated for all vertical levels in the ocean model, and only the value corresponding to the shelf draft is retained by the ice sheet model. When the ice sheet model cell is not covered by the ocean model, the value of the nearest ocean cell is retained.

The fluctuations in ice sheet volume have no impact on the global volume of the ocean in the model. As a result, sea level and bathymetry in the ocean model remain unchanged.

2.2 Experimental setup

2.2.1 Initial condition

We perform a long coupled ice sheet-climate simulation under constant external forcing at 40 ky B.P. to derive the initial state. This date precedes Heinrich stadial 4 and present relatively stable conditions regarding June insolation at 65 $^o N$. The climate model is forced with insolation (Berger, 1978) and greenhouse gases concentration (Lüthi et al., 2008). The ice sheet model is forced with sea level reconstruction (Waelbroeck et al., 2002). Forcings are held constant at their 40 ky B.P. values. The simulation starts from a previous equilibrium simulation of the Last Glacial Maximum (LGM) similar to the one described in Quiquet et al. (2021). We use a LGM bathymetry for the ocean model (Lhardy et al., 2021).

For this long spin-up simulation, we use an asynchronous coupling between the ice sheets and the rest of the climate system. Since the ice sheets feature slower dynamics than the ocean and the atmosphere, we run the ice sheet model for 10 years every year of the rest of the climate model. The spin-up simulation runs for 8,000 years for the ocean and the atmosphere but 80,000 years for the ice sheets. At the end of this simulation, the ice sheets and the rest of the climate is at equilibrium with a minimal ice mass change.

The ice sheet conditions at the end of the 40 ky equilibrium simulation are depicted in Figure 1. Ice is located over North America, Greenland, Iceland, Svalbard and Fennoscandia and corresponds rather well to the extent of the reconstructed ice
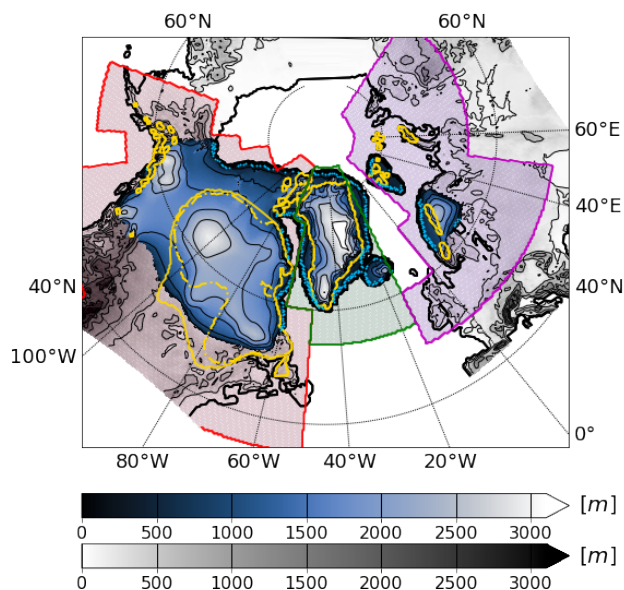
Figure 1. 40 k.y. equilibrium. Ice sheet elevation (shades of blue) and elevation above sea level (shades of gray) [m] at the end of the equilibrium simulation. Light blue contour is the mean position of the grounding line at the same time. Yellow contours are the minimal and maximal ice sheets extent in the reconstruction from Gowan et al. (2016), these differ only over the central North American ice sheet. Areas used to derive regional ice volumes on Figure 2 are shaded in red for North American, green for Greenland and Iceland and pink for Eurasian ice sheets.

sheet from Gowan et al. (2016). The reconstruction presents ice sheet volumes of around 12 and 16 million km^3 for minimal and maximal scenarios while we obtain a total volume of about 24 million km^3 of ice. This corresponds to 28 and 37 meters of equivalent sea-level (mSLE) for the reconstruction and 48 mSLE for this study. The difference is mainly due to larger Northern American ice sheet in our simulation.

2.2.2 Perturbation experiment

Each of the following experiment is branched on the 40 k.y. B.P. equilibrium. External forcings are still held constant at their 40 ky B.P. values. Differing from the spin-up simulation, here the climate and the ice sheets are annually coupled and freshwater fluxes are taken into account. The control experiment (CTRL) is the continuation of the equilibrium simulation decribed in 2.2.1 but with addition of freshwater flux to the ocean resulting from ice sheet melting. In the perturbation experiments, the dynamics of the ice sheets is disrupted by changes imposed on the ocean component. Each perturbation experiment consists of multiplying the oceanic basal melt rates (defined in Eq. 1) at each grid point by an amplification factor X, with X ranging from 5 to 300, for 500 years. From the ice sheets point of view, increasing the oceanic basal melt rates at time 0 is equivalent to imposing a subsurface warming yet this has no effect on initial ocean temperatures. Since we use a coupled setup, the ice
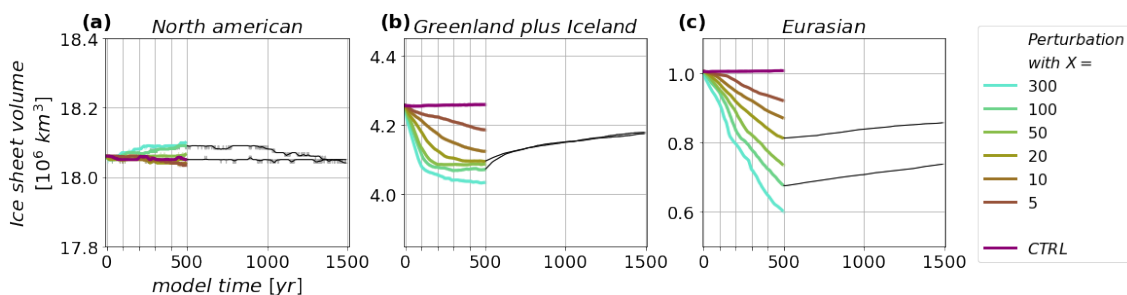
Figure 2. Continental ice volume response to oceanic perturbation (i.e. amplified OBM by a coefficient X). Time series of grounded ice sheet volume [10^6 km^3] for the (a) North American, (b) Greenland and Iceland and (c) Eurasian ice sheets in experiments with different perturbation factors. The thin black lines are the free evolution, once the perturbation is released, of the experiments where X = 20 and 100. Note that the same y-axis spacing is applied on the plots (0.6 10^6 km^3).

sheet retreat induced by our perturbation will impact the ocean through the resulting freshwater flux. Therefore in our perturbation experiments the freshwater feedback that could arise from the ocean-ice sheet interactions is taken into account, unlike traditional hosing experiments. The melt water is computed directly in the ice sheet model and transferred toward the nearest

135   ocean cell.

3   Results

3.1   Ice sheet response

The oceanic perturbation causes a decrease in the total volume of the Northern Hemisphere ice sheets. The relative contribu-

140   tions of the regional ice sheets show that the North American one contributes the least to the total volume change, while the Greenland, Iceland and Eurasian ice sheets contribute the most (Figure 2). The volume of the Greenland plus Iceland decreases rapidly over the first hundred years before reaching a new equilibrium for experiments with perturbation factors above 20. The Eurasian ice sheet loses volume throughout the perturbation period for all experiments. Once the perturbation is halted, Eurasian and Greenland plus Iceland regain mass at a slower pace. North American volume remains relatively unaffected by

145   the oceanic disturbance. For the highest perturbation factors, it even increases slightly till ~ 500 years and decrease once the perturbation is halted (Figure 2a).

   In the unperturbed state, the Hudson stream and Lancaster Sound form major ice streams for the North American (nomenclature follows Margold et al., 2015). There are also large velocities (above 500 m/yr) along the south east coast of Greenland and around Iceland (Figures 3a,b). Active regions with lower yet still above 100 m/yr velocities also include both Greenland

150   coasts and the Fennoscandian coast. The ice sheet evolution in the experiment with perturbation factor 100 (PERT100) is depicted in Figures 3c-f. After 200 years, the thinning is significant on the coasts bordering the Nordic Seas and to the south
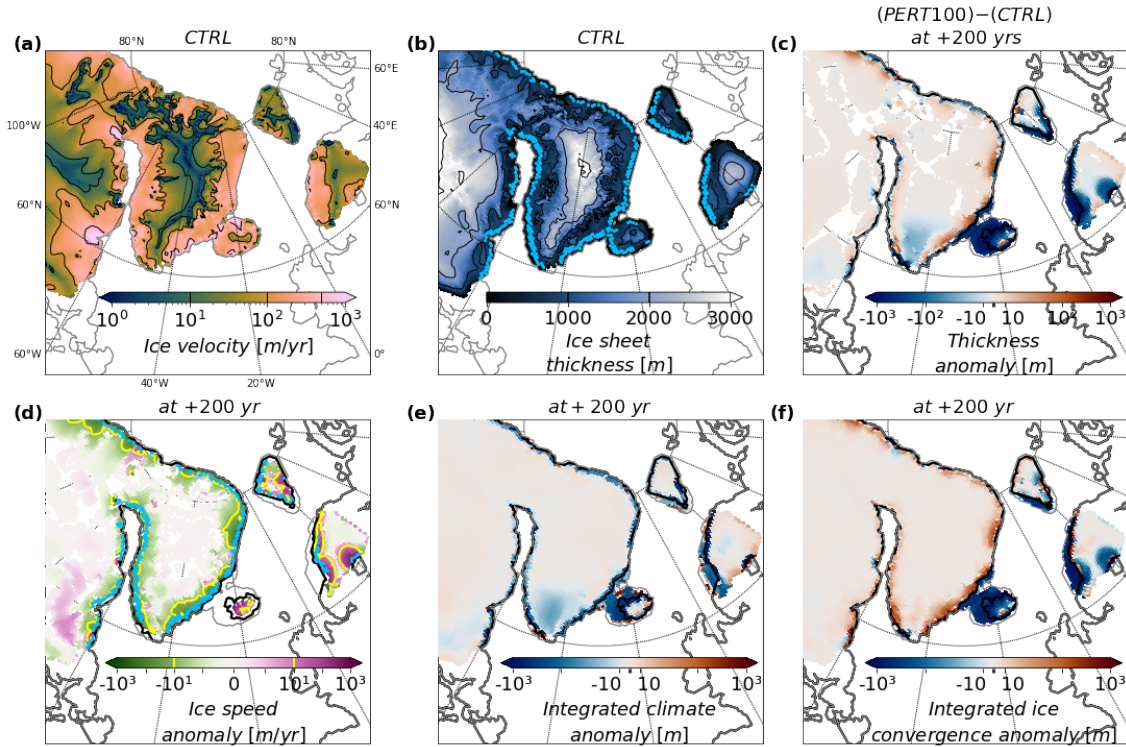
Figure 3. Ice sheet history in perturbation experiment with factor $X = 100$. Ice sheet (a) velocity [m/yr] and (b) thickness [m] averaged over the control simulation. Sky blue contour indicates the position of the grounding line. PERT100 - CTRL anomalies of (c) thickness, (d) ice velocities, (e) thickness due to climate anomalies, (f) due to ice convergence, after 200 years. Only significant values to one standard deviation of the control are shown for (c) and (d).

of the Greenland ice cap (Figure 3c), corroborating the volume time series (Figure 2). A smaller thinning is located inland to the south of Greenland. Upstream the coastal thinning, thickening takes place for the Greenland ice sheet, especially along the east coast. The latter is associated with the largest velocity decreases after 200 years (< -100 m/yr ; yellow contour on
155 Figure 3d). In contrast, ice flow velocities increased with the grounding line inland retreat on the Fennoscandian, Svalbard and Iceland coasts, sometimes until there is no more connection between ocean and land as it is the case for the Iceland after 200 years (blue contours ; Figures 3b versus d). To get further insight on the nature of the volume variations, we decompose the ice thickness changes such as (Eq. 2; mass conservation) :

$$H(t) - H(0) = \int_0^t (SMB - BM - C)dt - \int_0^t \boldsymbol{\nabla} \cdot (\boldsymbol{u}H)dt \qquad (2)$$

160 with H the ice thickness, SMB the surface mass balance, BM the basal melt rate, C the calving rate and $\boldsymbol{\nabla} \cdot (\boldsymbol{u}H)$ the ice flow divergence, dt is one year. We refer to the first term as climate term (although it contains the calving which is not strictly speaking a climate term). The residual is the lowering or thickening due to ice flow (dynamical effect).
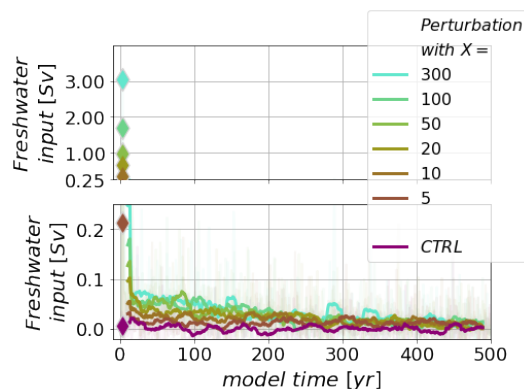
Figure 4. Time series of freshwater release [Sv] in experiments with different perturbation factor. Diamonds are the freshwater release for the first year of perturbation, light colors are the yearly outputs and saturated colors are smoothed time series (running mean over 21 years, centered).

The perturbation induces a loss of volume both through climate and dynamic thinning (Figure 3e,f). The oceanic melt rate perturbation is visible through negative thickness anomalies along the coasts on Figure 3e. The inland thinning over Greenland
165 is also caused by the climate term. The latter is due to change in surface mass balance (less accumulation over the Greenland when the fresh water is released; Figure S3).

The thickness decrease due to the dynamic term is most important in areas such as the west coast and southern part of the Fennoscandian (proglacial lake grounding line instability for the latter), the Svalbard, Iceland and southern tip of the Greenland ice sheet. The thickening in coastal areas appears in this term. The latter is counter-intuitive regarding the buttressing theories.
170 In the model, the flux at the grounding line connects thickness and velocities in the grounding zone through a power-law relationship (Tsai and Gudmundsson, 2015). Here, a reduction of the thickness due to the perturbation induces a reduction of the ice flux and upstream convergence (Figure 3f), so that the perturbation is not able to destabilize the ice sheet. This thickening effect also appears north of the North American ice sheet, at its connection with the Arctic ocean, and east at its connection with the Baffin Bay. Together with positive anomalies of the surface mass balance to the south, this contributes to
175 the small increase of the North American ice sheet for experiments with factors $X \geq 100$ (Figure 2a).

Still, the overall volume loss experienced by the ice sheets is equivalent to a freshwater release toward the ocean (Figure 4). The latter freshwater flux is particularly large during the first few years in all experiments and results from both increased calving and increased basal melt fluxes (not shown). Both are of the same order of magnitude: $\sim 1.25 * 10^{11}$ m^3/yr yet with different shapes. The calving flux increases quickly and drops toward the control value after 10 years while the basal melt flux
180 peaks and slowly decreases. This results in a freshwater flux that decreases (but remains significant) with time, suggesting the presence of ice sheet stabilizing mechanisms in the model. The larger the perturbation factor, the larger the freshwater volume added to the ocean.
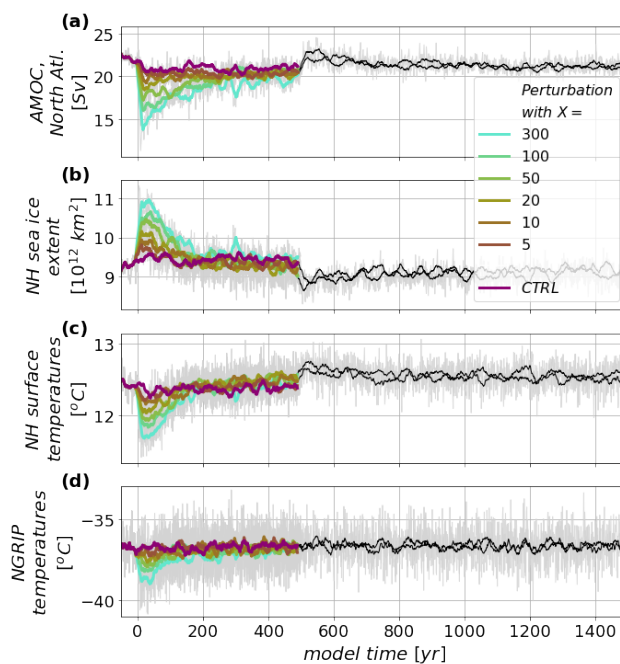
Figure 5. Times series of (a) AMOC intensity in the North Atlantic [Sv], (b) Northern Hemisphere sea ice extent [10^{12} km^2], (c) Northern Hemisphere and (d) NGRIP surface temperatures [^{o}C] in perturbation experiments with different factors. The thin black lines represent the unperturbed extension of the simulations with factors 20 and 100. Light colors are the yearly outputs and saturated colors are smoothed time series (running mean over 21 years, centered).

The freshwater release has the ability to modify climate, ocean hydrography and circulation which can in turn affect the ice sheets. In the following, we investigate climate and ocean changes and examine how they are connected with regional ice sheet changes.

3.2 Climate and ocean changes

Subsequent to the continental melt water release, the Atlantic meridional overturning circulation (AMOC) weakens for several years in all the simulations. There are no off modes in our simulations even with the largest perturbation factors. At the same time, the extent of the sea ice cover increases and the surface temperatures decrease over the Northern Hemisphere (Figure 5). The AMOC rapid decrease is followed by a slower recovery toward the control simulation values, corroborating the reduction of the freshwater inflow with time (Figure 4). Taking the example of the experiment with perturbation factor of 100, the maximum changes for the AMOC (-5 Sv in comparison with the control), the sea ice extent and the Northern Hemisphere temperature on smoothed time series are reached after 14 to 33 years.
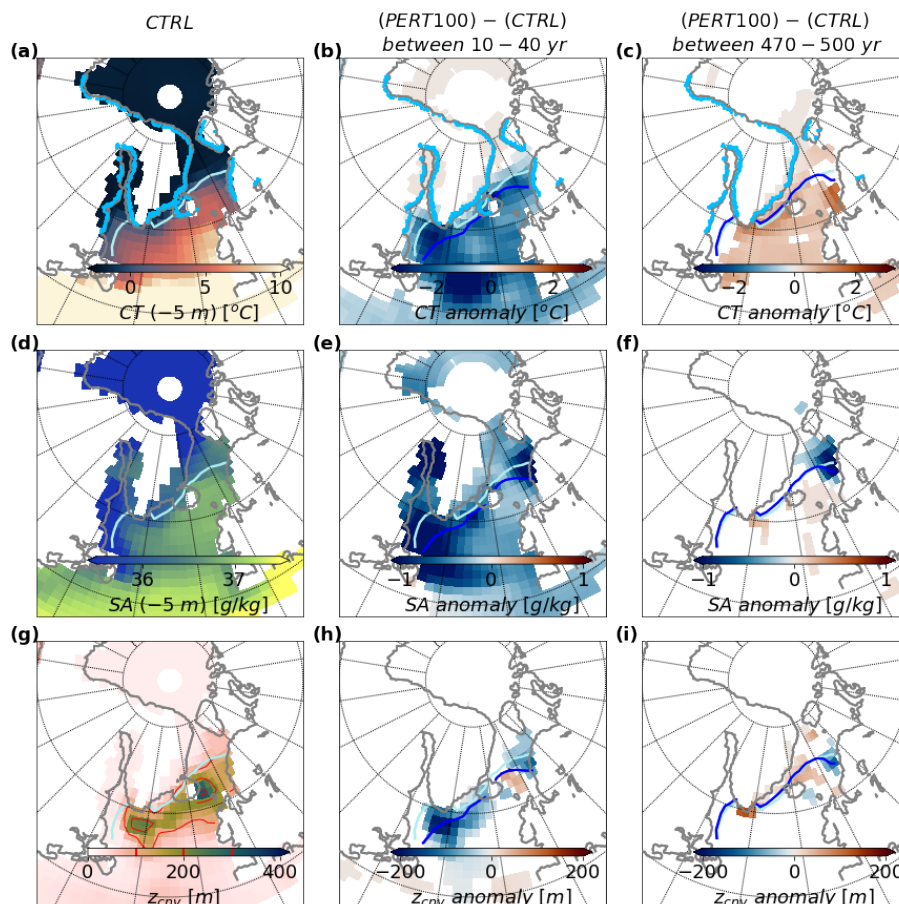
Climate
of the Past
Discussions

Figure 6. Hydrography at 5 meters depth horizon, in perturbation experiment with factor $X = 100$. Maps of (a)-(c) conservative temperature [^{o}C] over the control simulation and associated anomaly over 10-40 years and over 470-500 years comparing PERT100 and the control simulation. (d)-(f) Same for practical salinity [psu]. (g)-(i) Same for density [kg/m^3]. Only significant values to one standard deviation of the control simulation are shown for anomalies. Sky blue contour is the grounding line position in the control, after 40 years and after 500 years (resp. on a, b, c). Turquoise and dark blue contours are annual 30% sea ice contours in the control and the perturbation experiment, respectively.

195   In the unperturbed simulation, convective areas are located south of the sea-ice edge in the Labrador Sea and south of the Nordic Seas (Figure 6g). Following the freshwater release, major cooling and freshening occur at the surface and the sea ice extent moves southward (Figure 6a,b,d,e). This produces a decrease of the surface density over most of the convective sites resulting in convection reduction in the beginning of the perturbation period (Figure 6h) ; except east of Iceland where convection increases.

200   At the end of the perturbation period, the hydrographic variables almost returns to their control values and the ice-edge is close to the one of the control simulation. Nevertheless, the end of the perturbation period presents a slight warming at the
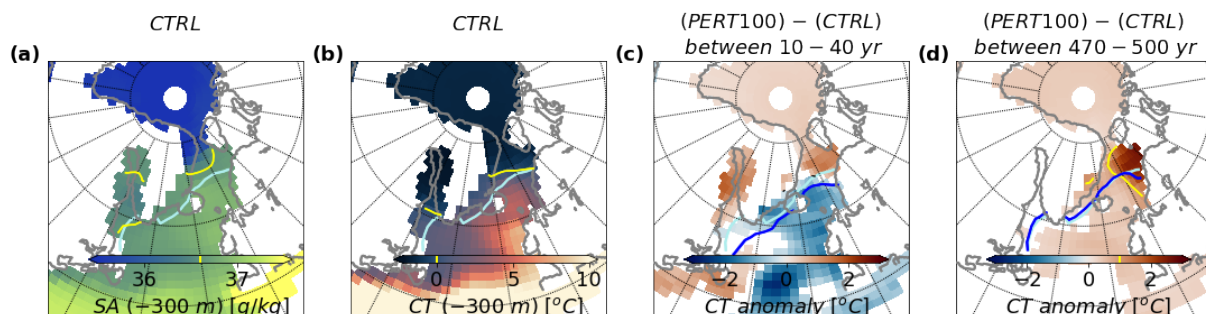
Figure 7. Hydrography at 300 meters depth horizon, in perturbation experiment with factor $X = 100$. Maps of (a) practical salinity [g/kg] and (b) conservative temperature [^oC] over the control simulation. Conservative temperatures anomalies (c) over 10-40 years and (d) over 470-500 years between the simulation with perturbation factor 100 and the control. Only significant values to one standard deviation of the control simulation are shown for anomalies. Yellow contours indicates 36.6 g/kg, 0 ^oC and $+1$ ^oC iso-contours (resp. on a,c,d). Turquoise and dark blue contours are annual 30% sea ice contours in the control and the perturbation experiment.

surface in the north east Atlantic and a negative salinity anomaly subsists at the surface in the northern Nordic Seas, while a slightly positive salinity anomaly is visible south of the sea-ice edge (Figure 6c,f).

South of the sea-ice edge, the positive temperature and salinity anomalies might be the result of the grounding lines retreat of the Fennoscandian and Iceland ice sheets (sky blue contours on Figures 6b,c), resulting in less inflow of cold and fresh water at the surface.

North of the sea-ice edge, the freshening pattern at the surface is caused by the accumulation of continental melt water through the duration of the perturbation (Figure 6f). Additionally, the weak meridional circulation at these latitudes does not promote the advection of the freshwater supply out of the area (Figure S4). The slight warming is driven from below, as suggested by temperature patterns at 300 m water depth (Figure 7c).

At 300 m depth (characteristic shelf draft), the subsurface warms in several locations following the freshwater release at the surface. These locations include the east and south of Newfoundland, the Baffin Bay, the north of the Greenland sea and the Arctic ocean. At the end of the perturbation, only the Nordic Seas warming remains significant with values above 1 ^oC. This area where the positive temperature anomaly has developed and amplified corresponds to the area where the ice flux is the most sustained over the perturbation period. The salinity also increases in the subsurface over the Nordic Seas with time, probably as the result of sea ice production and accumulation of saline Atlantic waters. The competing effects of temperature and salinity produce an overall density decrease at this depth that is smaller than at the surface (Figure S5). However, after 100 years, the vertical density gradient reverts from time to time due to accumulation of heat in the subsurface and the warm subsurface waters are mixed with surface waters during strong intermittent convective events (Figure S5,S6), leading to a positive surface temperature anomaly north of the sea-ice edge (Figure 6c).

In the Baffin Bay, despite subsurface warming at the beginning of the perturbation period, the situation is quite different and leads to less ice discharge. The reason for that could be found looking at background oceanic temperatures and salinity. Both these quantities are quite small by comparison to the same latitudes in the Nordic Seas (yellow contours Figures 7a, b).

225   Therefore, the amplified subsurface warming we apply to the ice sheets with multiplication by a factor 100 is not sufficient to perturb the ice sheet dynamics there.

3.3 Interactions between ice sheets and ocean

We perform another set of simulations, maintaining the oceanic perturbation and cutting off freshwater fluxes from the ice sheet model to the ocean model. This allows to highlight the freshwater release feedback on ice discharges. In other words, here the

230   ocean does not respond to the continental ice melt water and the oceanic feedback on the ice sheets is suppressed. Oceanic and atmospheric circulation could still vary from the control simulation, in response to changes in the ice sheet elevation (that could perturb the atmospheric physics and dynamics for instance) or extent of continental ice (that could induce albedo changes for instance).

When the freshwater fluxes are suppressed, the ice sheet response to the perturbation is amplified during the first few decades

235   with respect to the simulation where the freshwater fluxes are taken into account (Figures 8a,b). The Norwegian and Iceland ice sheets experience more losses (red areas; Figures 8c). In other areas such as the northern Labrador Sea (east coast of the Laurentide and west coast to the south of the Greenland ice sheets) an exacerbated thinning is also visible yet secondary.

To quantify and see the temporal evolution of the freshwater feedback on the ice sheets, we compute a feedback factor γ_X (Eq. 3).

$$240 \quad \gamma_X = \frac{\delta V_X - \delta V_{X,noFWF}}{\delta V_X} \tag{3}$$

Where δV_X is the continental ice volume variation with respect to time 0 in the simulation with perturbation factor X, $\delta V_{X,noFWF}$ in the associated simulation with no freshwater flux. This definition is adapted from Goosse et al. (2018), the difference being that here we do not consider equilibriums but transient states.

For the Greenland plus Iceland and Eurasian ice sheets, δV_X is negative (Figure 2). Thus, a negative γ_X means that

245    $0 > \delta V_X > \delta V_{X,noFWF}$ and indicates that there is more ice losses when the freshwater fluxes are not taken into account. Concerning the Greenland plus Iceland, the freshwater feedback on the volume variation is maximal in the beginning of the simulations (Figures 8a,b,d). After ~ 100 years, the ice evolution becomes stable in both experiments (Figures 2b, 8d). This is because of two different mechanisms : (1) Iceland grounding line retreats inland till there is no more connection with the ocean and no more sensitivity to the perturbation, (2) the applied perturbation is not sufficient to destabilize most of the Greenland

250   coasts, where initiated thinning leads to reduced velocities, upstream convergence and thickening. The resulting difference in thickness is slightly negative in the Greenland interior at the end of the simulations (blue patch; Figure 8e). As the thickness variation is also negative when the freshwater fluxes are taken into account, it means that there are less losses at this location when these are not taken into account. This is similar to what we have already described in section 3.1: the release of freshwater leads to less accumulation over the Greenland area.
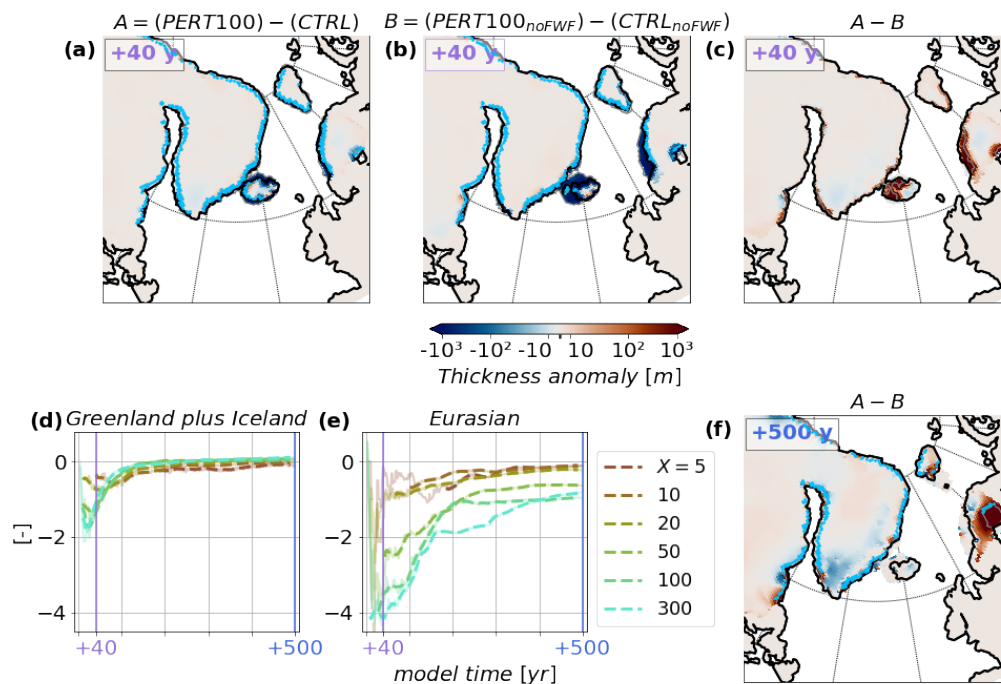
Figure 8. Thickness anomalies [m] between (a) perturbation experiment with factor $X = 100$ and the control simulation, (b) same with cut freshwater fluxes and (c) the difference between the two after 40 years and (f) after 500 years. Time series of (d) Greenland plus Iceland and (e) Eurasian feedback factor as defined in (Eq. 3) in the perturbation experiments. Light color lines are the yearly time series. Saturated color lines are smoothed time series (running mean over 21 years, centered) with values plotted when δV_X is above a critical value of $0.25 \; 10^{14}$ m^3.

255   Regarding the Eurasian ice sheet, the losses are amplified when the freshwater fluxes are not taken into account in the beginning of the simulation (Figure 8e). After ~ 200 years the time varying feedback factor becomes rather stable yet still negative for all perturbation experiments. This non-zero freshwater feedback signifies that the ice sheet volume is still decreasing in both cases, with and without freshwater fluxes, but at a larger rate for the second (Figures 2c and 8e). In both cases, the Fennoscandian ice sheet experiences a grounding line mechanical instability that implies mass loss.

260   Either way, ice volume decrease is faster when freshwater fluxes are not taken into account than when they are. Freshwater fluxes into the ocean bring water that is colder than the surrounding ocean and therefore help to maintain a cold water layer that extend from the surface to the ice shelf drafts. In addition, the local latent heat flux due to oceanic melting of the calved ice also helps to cool the upper part of the water column. All this act to temporarily protect the ice shelves from the underlying warm waters (Figure 7c). Nevertheless, the grounding line of the Iceland and Fennoscandian ice sheets eventually retreats
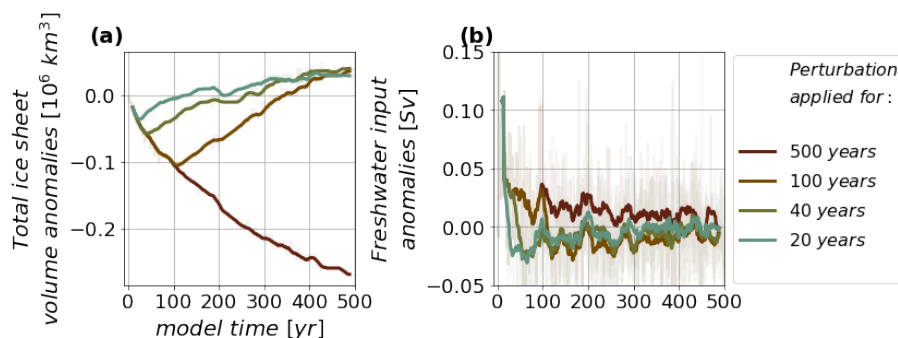
13

Figure 9. Time series of (a) grounded ice sheet volume anomalies [10^6 km^3] and (b) freshwater release anomalies [Sv] between experiments with imposed 10 m/yr ocean basal melt rates in the Baffin Bay for different periods and the control simulation.

completely in both simulations (blue contours; Figure 6c and Figure 8f). This suggests that freshwater fluxes are slowing down the grounding line retreat and dampening the ice volume losses rather than halting them.

4 Discussion

4.1 Laurentide ice sheet

The Hudson ice stream is often considered as a major source of massive iceberg discharges during the last glacial period (e.g., Andrews and Tedesco, 1992; Bond et al., 1992; Calov et al., 2002), while the Laurentide ice sheet is overall stable in our coupled experiments. This raises the question of whether this stability is an inherent characteristic of this ice sheet simulated by the coupled model or if the disturbance applied is insufficient to cause destabilization.

We have pointed that background temperatures are rather cold at the shelf drafts and salinity is low in the Baffin Bay and Labrador Sea to the south in comparison with the same latitudes in the eastern part of the North Atlantic. Background oceanic basal melt rates are thus lower (around 0.003 m/yr) at the mouth of the Hudson ice stream in the control simulation than around the Fennoscandian ice sheet (around 0.3 m/yr). Therefore, in our simulations, the oceanic perturbation with amplified basal melt rates is not able to destabilize the North American ice sheet/streams even with the highest multiplicative perturbation factor.

However, the warmer waters of Atlantic origin might have been transported by recirculations along the west coast of Greenland, reaching characteristic ice shelf depths, although our model cannot resolve such fine scales. So, we perform an other experiment with constant oceanic basal melt rate instead of multiplication of the background values to force ice sheet response in this area. We apply a constant rate of 10 m/yr over the Baffin Bay/Labrador Sea area for 500 years. This time, the disturbance affects the ice sheets volumes adjacent to the Baffin Bay/Labrador Sea area, the Laurentide and Greenland ice sheets (Figure S7). As the volume of the others ice sheets is stable in this experiment, the anomaly on the total volume is the anomaly due

285 to the perturbation. Here, in response to the applied oceanic melt rate, the total volume decreases (brown on Figure 9a). Fresh water is released to the ocean (brown on Figure 9b) through increased calving only during the first 10 years ($\sim 1.0 * 10^{11}$ m^3/yr) and increased melt at the shelves base ($\sim 0.25 * 10^{11}$ m^3/yr) all along the perturbation period (not shown).

In addition, we are investigating whether the release of freshwater can lead to subsurface warming and more destabilization of the ice sheets in this experiment. With the imposed constant melt rate, we have inhibited the model trajectory that the ice

290 sheets would follow. Therefore, here we also stop the perturbation after 20, 40 and 100 years and continue the simulation with free conditions. When the perturbation ceases the basal melt rates are always pulled back toward the control values (not shown) so does the freshwater input to the ocean and the total volume stops immediately to decrease (Figure 9). Once the perturbation is halted, the total volume grows again, even exceeding that of the control simulation. This regrowth is mainly due to dynamical convergence (Figure S7). In our simulation, the imposed initial subsurface warming of 10 m/yr is not amplified and the reduced

295 buttressing is not sufficient to lead to a sustained dynamic thinning upstream over this area.

4.2 Influence of the bathymetry choice on ice sheet sensitivity

The continental ice volume variations are modulated by the background temperature and salinity conditions and the ocean connection points with the marine terminated ice sheets. Temperatures and salinity are transported by currents, and the bathymetry plays a fundamental role in determining their geographical distribution. To ensure the robustness of our results concerning

300 freshwater feedback, we test an alternative bathymetry. Till now we used a bathymetry corresponding to the Last Glacial Maximum, here we do the same diagnosis but with a Pre-industrial bathymetry. The initial condition is built the same way as described in section 2.2.1. It leads to a sensibly different ice sheet with a lower total volume of about 22 million km^3 (44 mSLE). Differences in continental ice distribution include a North American ice sheet that reaches lower latitudes on its eastern side and a Fennoscandian ice sheet of smaller extent that is closer to the reconstruction of Gowan et al. (2016) (Figure S8).

305 Due to the differing geometries, the regions experiencing volume losses are not identical. The Greenland ice sheet loses significant volume along its southeastern coast, particularly at the beginning of the experiment (Figure S9). The Eurasian ice sheet has a smaller extent and reduced contact with the ocean, yet it still experiences substantial losses in its northern regions. The Laurentide ice sheet undergoes dynamical thinning with this geometry, but these losses are mostly confined to its southeastern region (Figure S9), where it is exposed to warmer waters (Figures S10-11).

310 This results in a total ice volume anomaly that is larger than with the LGM bathymetry : - 1.47 versus - 1.33 mSLE during the 500 years of perturbation. In this context, the weakening of the AMOC is amplified in comparison with the LGM bathymetry. With the Pre-industrial bathymetry the reduction is of around -7.5 Sv, from 26 to 18.5 Sv, while for the LGM the weakening is of -5 Sv, from 21 to 16 Sv.

However, the evolution of the feedback factor is very similar to what we obtained with the previous geometry. The ice volume

315 losses without freshwater input to the ocean are larger for both Greenland plus Iceland and Eurasian ice sheets, especially in the beginning of the experiment. Thus, the feedback factor is negative (Figure 10). Freshwater flow also dampens the volume losses of the North American ice sheet with the Pre-industrial bathymetry (Figure 10). After ~ 50 years, the volume of the North American ice sheet remains stable in the experiment with the freshwater fluxes while it continues to decrease with
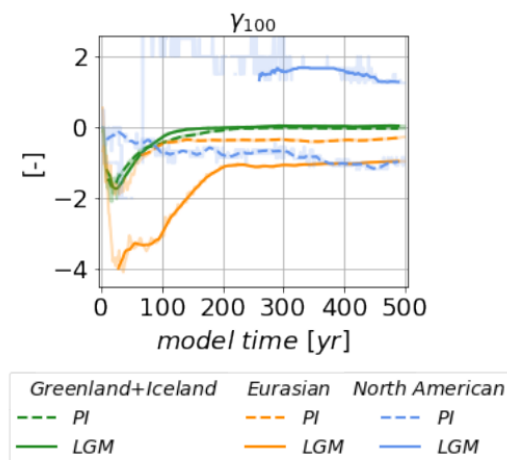
Figure 10. Time series of feedback factor as defined in (Eq. 3) in the perturbation experiments with factor X=100, with the Pre-industrial setup and the LGM setup, for the different ice sheets. Light color lines are the yearly time series. Saturated color lines are smoothed time series (running mean over 21 years, centered) with values plotted when δV_X is above a critical value of $0.25 \ 10^{14} \ \text{m}^3$.

suppressed freshwater fluxes (Figure S12). Note that γ_{100} is positive for the North American ice sheet with LGM bathymetry,
320 this accounts for the mass gain described in section 3.1.

4.3 Dansgaard-Oeschger and Heinrich events framework

Our simulations suggests that ocean subsurface warming could amplify stadial conditions. Indeed, the increase of oceanic basal melt rates leads to an increase of both calving fluxes and basal melt water release. The resulting freshwater release induces a temporary slowdown of the AMOC and decrease of the Northern Hemisphere temperature.

325 According to the air temperature record of Kindler et al. (2014), the onset of Heinrich stadial 4 corresponds to $6.5 \ ^oC$ temperature decrease and its end to a $10 \ ^oC$ increase at the NGRIP site. In comparison, our simulations present low temperature variation magnitudes, ranging between 0.5 and $2 \ ^oC$ for the smoothed time series (Figure 5d). In the model, Greenland temperature changes are mainly produced by AMOC changes. Following the onset of the perturbation and the inflow of freshwater, the AMOC intensity temporarily reduces but remains relatively high (Figure 5a). Consequently, Greenland temperatures also
330 remain relatively high, leading to small anomalies.

Moreover, the Laurentide ice sheet does not feature volume variations near the Hudson area, suggesting that the imposed perturbation in the case of amplified oceanic basal melt rates was too weak. This simulated behaviour of the Laurentide ice sheet is inconsistent with the paleo-data and the presence of ice rafted debris of Laurentide origin within the North Atlantic marine sediments (Broecker et al., 1992; Grousset et al., 2000). There are several possible reasons for this contradiction: (1) the
335 presence of cold biases in oceanic temperatures in the model (due to low model grid resolution and impossibility of resolving the circulation within the Baffin Bay, for example) or (2) the geometry of the ice sheet. Indeed, we have designed our initial

conditions based on the ice sheet reconstructions from Gowan et al. (2016). However, the Northern Hemisphere ice sheets are not well constrained before the Last Glacial Maximum. The use of alternative geometries, with continental ice free conditions over Hudson Bay, closer to other reconstructions for the same period (Dalton et al., 2022a, b), might produce different results. We note here that different modelling choices could lead to different responses for the Laurentide ice sheet. For instance, modelling choices affecting the basal dynamics of the ice sheet and its ability to slide over bedrock could lead to different results, as suggested by Hank and Tarasov (2024).

In addition, in the paleo-climatic records, Heinrich events are followed by an atmospheric warming over the Greenland ice sheet and North Atlantic region (Bond et al., 1993; Kindler et al., 2014), namely Dansgaard-Oeschger warming toward interstadial conditions. Here, our model results do not display such warming when the perturbation is released which is inconsistent with observations (Figure 5c,d). Some authors have suggested that increased sea ice formation during cold periods can lead to heat accumulation at the subsurface in the Nordic Seas (e.g., Rasmussen and Thomsen, 2004; Sadatzki et al., 2019). At some point, this accumulated heat destabilizes the water column, reversing the vertical density gradient. This reversal causes rapid oceanic mixing, bringing warm waters to the surface. The heat release to the atmosphere marks the onset of a Dansgaard-Oeschger interstadial (Dokken et al., 2013). In our simulation, the heat accumulated in the Nordic Seas (Figure 7) dissipates once the perturbation is released (Figure S13). Part of this heat is transferred to the atmosphere, as indicated by the sea-ice contour moving toward higher latitudes, the rising ocean surface temperatures during the first 30 years post-perturbation (Figure S13) and strong, intermittent convective events during the first hundred years after the perturbation ends (Figure S6). However, this has no imprint on Greenland temperatures. One possibility is that the heat reservoir is insufficient to counteract the rapid restratification that follows the surface heat release to the atmosphere (Figure S5), preventing the climate system from shifting to a new regime in our simulations. This could be explored in future studies.

5 Conclusions

In this study, we test the hypothesis that ocean subsurface warming triggers instabilities in Northern Hemisphere ice sheets. We use an Earth model of intermediate complexity (iLOVECLIM) coupled with an ice sheet model (GRISLI) and apply an oceanic perturbation at the shelves draft by multiplying the background oceanic basal melt rates with different factors. Our numerical experiments lead to several conclusions:

(1) The imposed amplified oceanic basal melt rates induces ice volume changes. Fresh water is released to the ocean through increased calving and oceanic basal melt water discharges. For most places the increased in oceanic basal melt rates leads to volume loss and dynamical thinning, while in some places the initial ice thickness decrease can lead to upstream dynamical thickening. Nevertheless, the influx of fresh water to the ocean induces a temporary increase in the sea-ice extent, a reduction in convection in the Labrador Sea, and hence a reduction in the Atlantic meridional overturning circulation and surface temperatures in the Northern Hemisphere as well as subsurface warming in the Nordic Seas.

370   (2) Cold and fresh water release dampens the ice sheet discharges (negative feedback).

(3) The Laurentide ice sheet volume does not vary and the Hudson stream is stable in our experiments with amplified basal melt rates. This can be explained by lower background temperature and salinity at shelf drafts in the Baffin Bay and Labrador Sea in comparison with the Nordic Seas. Imposing a constant perturbation of 10 m/yr in this area produces a volume decrease

375   of the adjacent ice sheets, yet it stops when the perturbation is halted.

To better contextualize this study within the framework of paleo-observations of massive iceberg discharges and Dansgaard-Oeschger events, it is also key to represent the rapid warming toward interstadial conditions following Heinrich events. The effects of the Antarctic ice sheet, which was prescribed in this study, could be examined. Indeed, the extent of the Antarctic

380   ice sheet may also fluctuate, leading to variations in the production of deep water around Antarctica (Paillard and Labeyriet, 1994). Accounting for these variations might result in more variability in the oceanic component than the present study. This is a potential area for future research. Lastly, our model can simulate carbon isotopes (Bouttes et al., 2015), allowing for direct comparison with observational data from marine sediment cores and providing additional constraints. This is another promising research direction.

References

Abot, L., Quiquet, A., and Waelbroeck, C.: Northern Hemisphere ice sheets and ocean interactions during the last glacial period in a coupled
ice sheet-climate model, [dataset]. Zenodo., https://doi.org/https://doi.org/10.5281/zenodo.12793237, 2024.

Alvarez-Solas, J., Charbit, S., Ritz, C., Paillard, D., Ramstein, G., and Dumas, C.: Links between ocean temperature and iceberg discharge
during Heinrich events, Nature Geoscience, 3, 122–126, https://doi.org/https://doi.org/10.1038/ngeo752, 2010.

Alvarez-Solas, J., Robinson, A., Montoya, M., and Ritz, C.: Iceberg discharges of the last glacial period driven by oceanic circulation changes,
Proceedings of the National Academy of Sciences, 110, 16 350–16 354, https://doi.org/https://doi.org/10.1073/pnas.1306622110, 2013.

Alvarez-Solas, J., Banderas, R., Robinson, A., and Montoya, M.: Ocean-driven millennial-scale variability of the Eurasian ice
sheet during the last glacial period simulated with a hybrid ice-sheet–shelf model, Climate of the Past, 15, 957–979,
https://doi.org/https://doi.org/10.5194/cp-15-957-2019, 2019.

Andrews, J. and Tedesco, K.: Detrital carbonate-rich sediments, northwestern Labrador Sea: Implications for ice-sheet dynamics
and iceberg rafting (Heinrich) events in the North Atlantic, Geology, 20, 1087–1090, https://doi.org/https://doi.org/10.1130/0091-
7613(1992)020<1087:DCRSNL>2.3.CO;2, 1992.

Arthur, F., Roche, D. M., Fyfe, R., Quiquet, A., and Renssen, H.: Simulations of the Holocene Climate in Europe Using Dynamical Downscal-
ing within the iLOVECLIM model (version 1.1), Climate of the Past, 19, 87–106, https://doi.org/https://doi.org/10.5194/cp-19-87-2023,
2023.

Barker, S., Chen, J., Gong, X., Jonkers, L., Knorr, G., and Thornalley, D.: Icebergs not the trigger for North Atlantic cold events, Nature,
520, 333–336, https://doi.org/https://doi.org/10.1038/nature14330, 2015.

Bassis, J. N., Petersen, S. V., and Mac Cathles, L.: Heinrich events triggered by ocean forcing and modulated by isostatic adjustment, Nature,
542, 332–334, https://doi.org/https://doi.org/10.1038/nature21069, 2017.

Berger, A.: Long-term variations of caloric insolation resulting from the Earth's orbital elements, Quaternary research, 9, 139–167,
https://doi.org/https://doi.org/10.1016/0033-5894(78)90064-9, 1978.

Bond, G., Heinrich, H., Broecker, W., Labeyrie, L., McManus, J., Andrews, J., Huon, S., Jantschik, R., Clasen, S., Simet, C., et al.:
Evidence for massive discharges of icebergs into the North Atlantic ocean during the last glacial period, Nature, 360, 245–249,
https://doi.org/https://doi.org/10.1038/360245a0, 1992.

Bond, G., Broecker, W., Johnsen, S., McManus, J., Labeyrie, L., Jouzel, J., and Bonani, G.: Correlations between climate records from North
Atlantic sediments and Greenland ice, Nature, 365, 143–147, https://doi.org/https://doi.org/10.1038/365143a0, 1993.

Bond, G. C. and Lotti, R.: Iceberg discharges into the North Atlantic on millennial time scales during the last glaciation, Science, 267,
1005–1010, https://doi.org/10.1126/science.267.5200.1005, 1995.

Bouttes, N., Roche, D. M., Mariotti, V., and Bopp, L.: Including an ocean carbon cycle model into iLOVECLIM (v1. 0), Geoscientific Model
Development, 8, 1563–1576, https://doi.org/https://doi.org/10.5194/gmd-8-1563-2015, 2015.

Bouttes, N., Swingedouw, D., Roche, D. M., Sanchez-Goni, M. F., and Crosta, X.: Response of the carbon cycle in an interme-
diate complexity model to the different climate configurations of the last nine interglacials, Climate of the Past, 14, 239–253,
https://doi.org/https://doi.org/10.5194/cp-14-239-2018, 2018.

Broecker, W., Bond, G., Klas, M., Clark, E., and McManus, J.: Origin of the northern Atlantic's Heinrich events, Climate Dynamics, 6,
265–273, https://doi.org/https://doi.org/10.1007/BF00193540, 1992.

Caley, T., Roche, D. M., and Renssen, H.: Orbital Asian summer monsoon dynamics revealed using an isotope-enabled global climate model, Nature communications, 5, 5371, https://doi.org/https://doi.org/10.1038/ncomms6371, 2014.

Calov, R., Ganopolski, A., Petoukhov, V., Claussen, M., and Greve, R.: Large-scale instabilities of the Laurentide ice sheet simulated in a fully coupled climate-system model, Geophysical Research Letters, 29, 69–1, https://doi.org/10.1029/2002GL016078, 2002.

Crameri, F.: Scientific colour maps (8.0.1), [dataset]. Zenodo., https://doi.org/https://doi.org/10.5281/zenodo.8409685, 2023.

Dalton, A. S., Pico, T., Gowan, E. J., Clague, J. J., Forman, S. L., McMartin, I., Sarala, P., and Helmens, K. F.: The marine δ18O record overestimates continental ice volume during Marine Isotope Stage 3, Global and Planetary Change, 212, 103814, https://doi.org/https://doi.org/10.1016/j.gloplacha.2022.103814, 2022a.

Dalton, A. S., Stokes, C. R., and Batchelor, C. L.: Evolution of the Laurentide and Innuitian ice sheets prior to the Last Glacial Maximum (115 ka to 25 ka), Earth-Science Reviews, 224, 103875, https://doi.org/https://doi.org/10.1016/j.earscirev.2021.103875, 2022b.

Dansgaard, W., Johnsen, S. J., Clausen, H. B., Dahl-Jensen, D., Gundestrup, N., Hammer, C. U., and Oeschger, H.: North Atlantic climatic oscillations revealed by deep Greenland ice cores, Climate processes and climate sensitivity, 29, 288–298, https://doi.org/https://doi.org/10.1029/GM029p0288, 1984.

Dansgaard, W., Johnsen, S. J., Clausen, H. B., Dahl-Jensen, D., Gundestrup, N. S., Hammer, C. U., Hvidberg, C. S., Steffensen, J. P., Sveinbjörnsdottir, A. E., Jouzel, J., et al.: Evidence for general instability of past climate from a 250-kyr ice-core record, nature, 364, 218–220, https://doi.org/https://doi.org/10.1038/364218a0, 1993.

Dokken, T. M., Nisancioglu, K. H., Li, C., Battisti, D. S., and Kissel, C.: Dansgaard-Oeschger cycles: Interactions between ocean and sea ice intrinsic to the Nordic seas, Paleoceanography, 28, 491–502, https://doi.org/10.1002/palo.20042., 2013.

Elliot, M., Labeyrie, L., Bond, G., Cortijo, E., Turon, J.-L., Tisnerat, N., and Duplessy, J.-C.: Millennial-scale iceberg discharges in the Irminger Basin during the last glacial period: Relationship with the Heinrich events and environmental settings, Paleoceanography, 13, 433–446, https://doi.org/https://doi.org/10.1029/98PA01792, 1998.

Favier, L., Jourdain, N. C., Jenkins, A., Merino, N., Durand, G., Gagliardini, O., Gillet-Chaulet, F., and Mathiot, P.: Assessment of sub-shelf melting parameterisations using the ocean–ice-sheet coupled model NEMO (v3. 6)–Elmer/Ice (v8. 3), Geoscientific Model Development, 12, 2255–2283, https://doi.org/https://doi.org/10.5194/gmd-12-2255-2019, 2019.

Fichefet, T. and Maqueda, M. M.: Sensitivity of a global sea ice model to the treatment of ice thermodynamics and dynamics, Journal of Geophysical Research: Oceans, 102, 12609–12646, https://doi.org/https://doi.org/10.1029/97JC00480, 1997.

Goosse, H., Brovkin, V., Fichefet, T., Haarsma, R., Huybrechts, P., Jongma, J., Mouchet, A., Selten, F., Barriat, P.-Y., Campin, J.-M., et al.: Description of the Earth system model of intermediate complexity LOVECLIM version 1.2, Geoscientific Model Development, 3, 603–633, https://doi.org/https://doi.org/10.5194/gmd-3-603-2010, 2010.

Goosse, H., Kay, J. E., Armour, K. C., Bodas-Salcedo, A., Chepfer, H., Docquier, D., Jonko, A., Kushner, P. J., Lecomte, O., Massonnet, F., et al.: Quantifying climate feedbacks in polar regions, Nature communications, 9, 1919, https://doi.org/https://doi.org/10.1038/s41467-018-04173-0, 2018.

Gowan, E. J., Tregoning, P., Purcell, A., Montillet, J.-P., and McClusky, S.: A model of the western Laurentide Ice Sheet, using observations of glacial isostatic adjustment, Quaternary Science Reviews, 139, 1–16, https://doi.org/https://doi.org/10.1016/j.quascirev.2016.03.003, 2016.

Grousset, F. E., Pujol, C., Labeyrie, L., Auffret, G., and Boelaert, A.: Were the North Atlantic Heinrich events triggered by the behavior of the European ice sheets?, Geology, 28, 123–126, 2000.

Gudmundsson, G. H., Paolo, F. S., Adusumilli, S., and Fricker, H. A.: Instantaneous Antarctic ice sheet mass loss driven by thinning ice shelves, Geophysical Research Letters, 46, 13 903–13 909, https://doi.org/https://doi.org/10.1029/2019GL085027, 2019.

Hank, K. and Tarasov, L.: The comparative role of physical system processes in Hudson Strait ice stream cycling: a comprehensive model-based test of Heinrich event hypotheses, EGUsphere, 2024, 1–36, https://doi.org/https://doi.org/10.5194/egusphere-2024-493, 2024.

470　Holland, D. M., Nicholls, K. W., and Basinski, A.: The southern ocean and its interaction with the Antarctic ice sheet, Science, 367, 1326–1330, https://doi.org/10.1126/science.aaz5491, 2020.

Holland, P. R., Jenkins, A., and Holland, D. M.: The response of ice shelf basal melting to variations in ocean temperature, Journal of Climate, 21, 2558–2572, https://doi.org/https://doi.org/10.1175/2007JCLI1909.1, 2008.

Johnsen, S. J., Clausen, H. B., Dansgaard, W., Fuhrer, K., Gundestrup, N., Hammer, C. U., Iversen, P. l., Jouzel, J., Stauffer, B., et al.: Irregular

475　glacial interstadials recorded in a new Greenland ice core, Nature, 359, 311–313, https://doi.org/https://doi.org/10.1038/359311a0, 1992.

Johnson, G. C. and Lyman, J. M.: Warming trends increasingly dominate global ocean, Nature Climate Change, 10, 757–761, https://doi.org/https://doi.org/10.1038/s41558-020-0822-0, 2020.

Joughin, I. and Alley, R. B.: Stability of the West Antarctic ice sheet in a warming world, Nature Geoscience, 4, 506–513, https://doi.org/https://doi.org/10.1038/ngeo1194, 2011.

480　Kindler, P., Guillevic, M., Baumgartner, M., Schwander, J., Landais, A., and Leuenberger, M.: Temperature reconstruction from 10 to 120 kyr b2k from the NGRIP ice core, Climate of the Past, 10, 887–902, https://doi.org/https://doi.org/10.5194/cp-10-887-2014, 2014.

Le Meur, E. and Huybrechts, P.: A comparison of different ways of dealing with isostasy: examples from modelling the Antarctic ice sheet during the last glacial cycle, Annals of glaciology, 23, 309–317, https://doi.org/https://doi.org/10.3189/S0260305500013586, 1996.

Lhardy, F., Bouttes, N., Roche, D. M., Crosta, X., Waelbroeck, C., and Paillard, D.: Impact of Southern Ocean surface conditions on deep

485　ocean circulation during the LGM: a model analysis, Climate of the Past, 17, 1139–1159, https://doi.org/10.5194/cp-17-1139-2021, 2021.

Li, D., DeConto, R. M., Pollard, D., and Hu, Y.: Competing climate feedbacks of ice sheet freshwater discharge in a warming world, Nature Communications, 15, 5178, https://doi.org/https://doi.org/10.1038/s41467-024-49604-3, 2024.

Lüthi, D., Le Floch, M., Bereiter, B., Blunier, T., Barnola, J.-M., Siegenthaler, U., Raynaud, D., Jouzel, J., Fischer, H., Kawamura, K., et al.: High-resolution carbon dioxide concentration record 650,000–800,000 years before present, nature, 453, 379–382,

490　https://doi.org/https://doi.org/10.1038/nature06949, 2008.

Marcott, S. A., Clark, P. U., Padman, L., Klinkhammer, G. P., Springer, S. R., Liu, Z., Otto-Bliesner, B. L., Carlson, A. E., Ungerer, A., Padman, J., et al.: Ice-shelf collapse from subsurface warming as a trigger for Heinrich events, Proceedings of the National Academy of Sciences, 108, 13 415–13 419, https://doi.org/https://doi.org/10.1073/pnas.1104772108, 2011.

Margold, M., Stokes, C. R., and Clark, C. D.: Ice streams in the Laurentide Ice Sheet: Identification, characteristics and comparison to

495　modern ice sheets, Earth-Science Reviews, 143, 117–146, https://doi.org/https://doi.org/10.1016/j.earscirev.2015.01.011, 2015.

Max, L., Nürnberg, D., Chiessi, C. M., Lenz, M. M., and Mulitza, S.: Subsurface ocean warming preceded Heinrich Events, Nature Communications, 13, 4217, https://doi.org/10.1038/s41467-022-31754-x, 2022.

Millero, F.: Freezing point of sea water, eighth report of the Joint Panel of Oceanographic Tables and Standards, appendix, 6, 29–31, 1978.

Moorman, R., Morrison, A. K., and McC. Hogg, A.: Thermal responses to Antarctic ice shelf melt in an eddy-rich global ocean–sea ice

500　model, Journal of Climate, 33, 6599–6620, https://doi.org/10.1175/JCLI-D-19-0846.1, 2020.

Naughten, K. A., Holland, P. R., and De Rydt, J.: Unavoidable future increase in West Antarctic ice-shelf melting over the twenty-first century, Nature Climate Change, 13, 1222–1228, https://doi.org/https://doi.org/10.1038/s41558-023-01818-x, 2023.

Climate
of the Past
Discussions

Paillard, D. and Labeyriet, L.: Role of the thermohaline circulation in the abrupt warming after Heinrich events, Nature, 372, 162–164, https://doi.org/https://doi.org/10.1038/372162a0, 1994.

505 Pollard, D.: A simple parameterization for ice sheet ablation rate, Tellus, 32, 384–388, https://doi.org/https://doi.org/10.3402/tellusa.v32i4.10593, 1980.

Pritchard, H., Ligtenberg, S. R., Fricker, H. A., Vaughan, D. G., van den Broeke, M. R., and Padman, L.: Antarctic ice-sheet loss driven by basal melting of ice shelves, Nature, 484, 502–505, https://doi.org/https://doi.org/10.1038/nature10968, 2012.

Quiquet, A., Dumas, C., Ritz, C., Peyaud, V., and Roche, D. M.: The GRISLI ice sheet model (version 2.0): calibration
510 and validation for multi-millennial changes of the Antarctic ice sheet, Geoscientific Model Development, 11, 5003–5025, https://doi.org/https://doi.org/10.5194/gmd-11-5003-2018, 2018.

Quiquet, A., Roche, D. M., Dumas, C., Bouttes, N., and Lhardy, F.: Climate and ice sheet evolutions from the last glacial maximum to the pre-industrial period with an ice-sheet–climate coupled model, Climate of the Past, 17, 2179–2199, https://doi.org/https://doi.org/10.5194/cp-17-2179-2021, 2021.

515 Rasmussen, T. L. and Thomsen, E.: The role of the North Atlantic Drift in the millennial timescale glacial climate fluctuations, Palaeogeography, Palaeoclimatology, Palaeoecology, 210, 101–116, https://doi.org/https://doi.org/10.1016/j.palaeo.2004.04.005, 2004.

Reese, R., Gudmundsson, G. H., Levermann, A., and Winkelmann, R.: The far reach of ice-shelf thinning in Antarctica, Nature Climate Change, 8, 53–57, https://doi.org/10.1038/s41558-017-0020-x, 2018.

Ritz, C., Rommelaere, V., and Dumas, C.: Modeling the evolution of Antarctic ice sheet over the last 420,000 years: Im-
520 plications for altitude changes in the Vostok region, Journal of Geophysical Research: Atmospheres, 106, 31 943–31 964, https://doi.org/https://doi.org/10.1029/2001JD900232, 2001.

Roche, D. M., Dumas, C., Bügelmayer, M., Charbit, S., and Ritz, C.: Adding a dynamical cryosphere to iLOVECLIM (version 1.0): coupling with the GRISLI ice-sheet model, Geoscientific Model Development, 7, 1377–1394, https://doi.org/https://doi.org/10.5194/gmd-7-1377-2014, 2014.

525 Sadatzki, H., Dokken, T. M., Berben, S. M., Muschitiello, F., Stein, R., Fahl, K., Menviel, L., Timmermann, A., and Jansen, E.: Sea ice variability in the southern Norwegian Sea during glacial Dansgaard-Oeschger climate cycles, Science advances, 5, eaau6174, https://doi.org/10.1126/sciadv.aau6174, 2019.

Shaffer, G., Olsen, S. M., and Bjerrum, C. J.: Ocean subsurface warming as a mechanism for coupling Dansgaard-Oeschger climate cycles and ice-rafting events, Geophysical Research Letters, 31, https://doi.org/https://doi.org/10.1029/2004GL020968, 2004.

530 Swingedouw, D., Fichefet, T., Huybrechts, P., Goosse, H., Driesschaert, E., and Loutre, M.-F.: Antarctic ice-sheet melting provides negative feedbacks on future climate warming, Geophysical Research Letters, 35, https://doi.org/https://doi.org/10.1029/2008GL034410, 2008.

Tabone, I., Robinson, A., Alvarez-Solas, J., and Montoya, M.: Impact of millennial-scale oceanic variability on the Greenland ice-sheet evolution throughout the last glacial period, Climate of the Past, 15, 593–609, https://doi.org/https://doi.org/10.5194/cp-15-593-2019, 2019.

535 Tsai, V. C. and Gudmundsson, G. H.: An improved model for tidally modulated grounding-line migration, Journal of Glaciology, 61, 216–222, https://doi.org/https://doi.org/10.3189/2015JoG14J152, 2015.

Van Achter, G., Fichefet, T., Goosse, H., Pelletier, C., Haubner, K., and Pattyn, F.: Ocean–Ice Sheet Coupling in the Totten Glacier Area, East Antarctica: Analysis of the Feedbacks and Their Response to a Sudden Ocean Warming, Geosciences, 13, 106, https://doi.org/https://doi.org/10.3390/geosciences13040106, 2023.

540 Van Den Berg, J., van de Wal, R., and Oerlemans, H.: A mass balance model for the Eurasian Ice Sheet for the last 120,000 years, Global and Planetary Change, 61, 194–208, 2008.

Waelbroeck, C., Labeyrie, L., Michel, E., Duplessy, J.-C., Mcmanus, J. F., Lambeck, K., Balbon, E., and Labracherie, M.: Sea-level and deep water temperature changes derived from benthic foraminifera isotopic records, Quaternary science reviews, 21, 295–305, https://doi.org/https://doi.org/10.1016/S0277-3791(01)00101-9, 2002.

545 Wekerle, C., McPherson, R., von Appen, W.-J., Wang, Q., Timmermann, R., Scholz, P., Danilov, S., Shu, Q., and Kanzow, T.: Atlantic Water warming increases melt below Northeast Greenland's last floating ice tongue, Nature Communications, 15, 1336, https://doi.org/https://doi.org/10.1038/s41467-024-45650-z, 2024.